Mon. Not. R. Astron. Soc. **317**, 299–309 (2000)

Abundances in Przybylski's star

C. R. Cowley,[1] T. Ryabchikova,[2,3] F. Kupka,[4★] D. J. Bord,[5] G. Mathys[6] and W. P. Bidelman[7]

[1]*Department of Astronomy, University of Michigan, David M. Dennison Building, Ann Arbor, MI 48109, USA*
[2]*Institute of Astronomy, Russian Academy of Sciences, Pyatnitskaya str. 48, 109017 Moscow, Russia*
[3]*Visiting Scientist, Institute of Astronomy, University of Vienna, Türkenschanzstraße 17, A-1180 Vienna, Austria*
[4]*Institute for Astronomy, University of Vienna, Türkenschanzstraße 17, A-1180 Vienna, Austria*
[5]*Department of Natural Sciences, The University of Michigan-Dearborn, 4901 Evergreen Rd., Dearborn, MI 48128-1491, USA*
[6]*European Southern Observatory, Casilla 19001, Santiago 19, Chile*
[7]*Case Western Reserve University, Department of Astronomy, Cleveland, OH 44106-7215, USA*

Accepted 2000 February 26. Received 2000 February 25; in original form 1999 December 15

ABSTRACT

We have derived abundances for 54 elements in the extreme roAp star HD 101065. ESO spectra with a resolution of about 80 000, and S/N of 200 or more were employed. The adopted model has $T_{\rm eff} = 6600$ K, and $\log(g) = 4.2$. Because of the increased line opacity and consequent low gas pressure, convection plays no significant role in the temperature structure. Lighter elemental abundances through the iron group scatter about standard abundance distribution (SAD) (solar) values. Iron and nickel are about one order of magnitude deficient while cobalt is enhanced by 1.5 dex. Heavier elements, including the lanthanides, generally follow the solar pattern but enhanced by 3 to 4 dex. Odd-Z elements are generally less abundant than their even-Z neighbours. With a few exceptions (e.g. Yb), the abundance pattern among the heavy elements is remarkably coherent, and resembles a displaced solar distribution.

Key words: stars: abundances – stars: chemically peculiar – stars: individual: HD 101065.

1 INTRODUCTION

About a year ago, two of us (Cowley & Mathys 1998, hereafter Paper I) discussed a modern analysis of the spectrum of Przybylski's star (HD 101065, V816 Cen). The unusual nature of this spectrum was first noted by A. Przybylski (1961). It is the only stellar spectrum known in which the second lanthanide spectra so dominate that even the presence of lines from iron-group elements has been controversial. Przybylski maintained for some time that Fe I was absent in the spectrum, although he eventually wrote to CRC (Przybylski, private communication) that he saw 'no reason to oppose' conclusions that Fe I was weakly present.

Paper I supported the claims made decades ago by Wegner & Petford (1974) and elaborated by Wegner, Kurtz, and their coworkers (cf. Kurtz 1990). HD 101065 appears to be a cool, extreme member of the family of rapidly oscillating Ap stars now called roAps. Its bizarre spectrum is the result of its relatively low temperature, combined with extreme excesses of rare-earth elements (REEs). However, we found these excesses (3–4 dex) were about the same as those assigned to the hot Ap stars in Hack's (1976) review. Some historical details, including a summary of the debate over the nature of Przybylski's star, may be found at the URL http://www.astro.lsa.umich.edu/users/cowley/przyb.html. This URL also contains links to wavelength identification lists, equivalent width measurements, and the corresponding oscillator strengths used in the present paper.

The spectral region available to us in the preliminary study was from $\lambda\lambda$5445 to 6587 with a resolution of about 18 000. While this material was superior to that of the photographic spectra of Przybylski, or Wegner and Petford, we were still unable to identify the controversial iron-group spectra at truly high confidence levels, although Wegner et al. (1983) have identified many lines of the singly-ionized iron-group elements in the IUE spectra of HD 101065 using classical methods. It should be added that Bord & Desko (1986) analysed the same IUE material with WCS and confirmed the presence of Fe I and Fe II lines at a high confidence level. The extended debate between Przybylski on the one hand and Wegner and his collaborators on the other over the mere presence of Fe I illustrates how subjective traditional line identification methods can be. To get beyond subjectivity, we required an impersonal technique, such as the method of wavelength coincidence statistics (WCS) and still higher resolution data.

2 NEW OBSERVATIONS AND PRELIMINARY REDUCTIONS

A new spectrum of HD 101065 was obtained by GM in February

★ E-mail: kupka@astro.univie.ac.at

© 2000 RAS

1998 with the 3.5-m New Technology Telescope at La Silla. The ESO Multi-Mode instrument was used in its cross-dispersed echelle mode to achieve a resolving power of about 80 000. This material covers the region from λλ3959 to 6652. Three exposures of 35 min each were obtained. They were combined in the reduction process, with application of a median filter to remove cosmic ray hits. Data processing was carried out with MIDAS. The spectrum was flat fielded prior to extraction. In the reduced spectrum, a S/N ratio of 200 or better was achieved. For wavelength calibration, a 2D-fit procedure similar to that described by Mathys & Hubrig (1997) was preferred to the standard MIDAS approach.

The one-dimensional, rectified spectra were measured and analysed at Michigan by DJB and CRC using the suite of programs used in Paper I. These codes require fluxes at equidistant intervals of 0.02 or 0.002 Å (the latter for solar work). The fluxes were displayed 512 points at a time (5.11 Å), and a cursor set at the minima of symmetrical lines. For blends, two or more measurements might be made, based on a subjective judgement of where the individual centroids and minima might be. Both wavelengths and intensity minima were recorded for 7964 features.

Independently, the spectral region λλ5000–6630 was measured in Moscow with the help of MultiProfile (MP, Smirnov & Ryabchikova 1995). The whole spectrum is approximated by a sum of Gaussian profiles, and we obtain central wavelength, line depth, full width at half maximum, and equivalent width for each measured feature. After being corrected to the rest frame, both sets of wavelength measurements agree within 0.005 Å. With MP, we measured about 5500 spectral features in the λλ5000–6620 spectral region. In the same region, 4158 features were measured by CRC. The automated procedure was somewhat more intensive (see Section 3.1 below).

It is of some interest to compare the current material with that discussed by Bidelman, Cowley & Iler (1995) for the rare-earth maximum of HR 465. Within overlapping regions from about λ3959.5 to λ4731.5, 2743 wavelengths were measured for HD 101065, while 1850 were measured for HD 465. The line density is significantly higher in HD 101065. The spectra are not of the same quality, however, so that the relative *intrinsic* line density is not known.

3 WAVELENGTH IDENTIFICATIONS

WCS studies showed that La II, Ce II, Nd II, Sm II, Gd II, Dy II and Er II are all extraordinarily well represented in HD 101065. We concluded that *more* lines of these ions were present in the stellar spectrum than in the well-known monograph of Meggers, Corliss & Scribner (1975, hereafter Monograph 145). This conclusion was supported in two ways. First, WCS trials showed persistently high significances, even when the faintest lines from Monograph 145 were used in the tests. Secondly, significant WCS results were obtained when sets of weak lines were used from Ce II (Corliss 1973), Sm II (Schweighofer 1970), Gd II (King 1943) and Dy II (Conway & Worden 1970) from which all Monograph 145 lines were purged.

On the strength of these results, we automated a part of the wavelength identification procedure. All lines from the seven species mentioned above that are in Monograph 145 were assigned as identifications or partial contributors to measured wavelengths in HD 101065 provided the stellar and laboratory lines were within 0.06 Å. This tolerance is a somewhat arbitrary choice, but it is based on experience with WCS and spectroscopic material with resolution near 40 000. There is no doubt that some lines that are further from the measured position than 0.06 Å make a significant contribution to a few stellar features, but assignments in such cases were made in the traditional way. The majority of the identifications were made in the automated fashion.

Identifications from Paper I were transferred to the corresponding features of the new spectra. These additional identifications consisted primarily of a few iron-group spectra, third spectra of the lanthanides and some Y II lines.

In the blue–violet region (λλ3959–4950) a major effort was made by WPB to identify as many features as possible. The net result is that the fraction of unidentified features in this region (44 per cent) is significantly lower than in the visual (λλ5000–6632, 66 per cent). Similar identification work has been completed for the visual region but is not yet available in digital form.

Line identifications were checked by synthetic spectrum calculations performed by TR for the λλ4500–6620 spectral region. Several additional species were identified; they are included in Table 3 below. We used abundances from Paper I as starting values, and assumed an overabundance up to 4 dex for all elements heavier than nickel. The necessary information for our spectral synthesis were extracted from VALD–2 (Kupka et al. 1999). Synthetic spectra also gave us the possibility of choosing mostly unblended lines for subsequent analysis, and to add a few elements to those with features available for abundances.

All calculations were carried out with SYNTH (Piskunov 1992).

Identification lists are available via links from the above URL.

3.1 Faint lines

A highly subjective judgement is involved in the decision to measure – or not to measure – a feature close to the continuum. CRC has adopted a policy of making 'intensive' measurements of stellar lines and has tried to measure any feature we think *might* be real. A different approach was used by TR. In principle, MultiProfile allows one to measure a noise level for any spectral region if we have a proper spectral window with a pure continuum. It is difficult to find continuum windows in HD 101065, therefore we accepted $S/N = 200$ ($\sigma = 0.05$), and MultiProfile automatically considers every feature as a real line if it has a depth of $\geqslant 2\sigma$.

In Paper I, we decided to purge the weakest features from our final list because WCS tests based on these lines alone failed to give any statistically significant identifications beyond those expected by chance. With the new material, we have an opportunity to see if this judgement was realistic.

A WCS test was made using the intensity-zero lines from Paper I as though they were an atomic species. The null hypothesis would be that there was no relation between the two sets of measurements. A test based on 200 random trials with the 222 intensity-zero lines from Paper I showed that the null hypothesis could be rejected at the 13 sigma level! Those zero intensity lines definitely contained information.

We can be sure that measurable features in the new spectra go below the intensity threshold of Monograph 145 for the ubiquitous second lanthanide spectra. It is therefore reasonable to attribute a significant fraction of the intensity-zero lines of Paper I to faint lines, mostly from the second spectra of the lanthanides. Most of these lines would have been above the threshold in the newer material, and systematically measured.

We have not purged intensity-zero lines from the current lists.

Table 1. The richest spectra (significance >4).

Spectra	Significance	Spectra	Significance
Ti I	4.73	Pr III	6.53
Ti II	4.55	Nd II	16.37
Fe I	6.02	Sm II	11.42
Fe II	4.19	Eu II	4.64
Co I	7.28	Gd II	10.17
Y II	4.68	Dy II	8.53
La II	10.36	Er II	10.19
Ce II	15.53	Tm II	5.46
Pr II	6.71		

Table 2. Other securely identified species. Significance is given for values greater than 1, Monte Carlo probability of null hypothesis or remarks otherwise (see text for details).

Spectra	Significance (or other criteria)	Spectra	Significance (or other criteria)
H I	$\alpha, \beta, \gamma, \ldots,$	Pd I	0.02+6 ID'd lines
Na I	D-lines	Y I	0.01
Si I	3.01	Zr II	3.06
Si II	0.005	Nb II	3.60
Ca I	3.99	Ba II	Mult. 1, 2
Ca II	H and K	Nd III	Strong lines
V II	2.59	Tb II	0.035
Cr I	2.92	Tb III	0.045
Cr II	3.29	Yb II	2.78
Sr II	4215 (not str!)	Lu II	3.82

3.2 Summary of identifications

The following tables contain summaries of the results of the WCS surveys, traditional identification methods (WPB) and the synthesis technique (TR). In WCS, the 'Significance' parameter is given in Tables 1 and 2. It measures the confidence, in standard deviations, with which the null hypothesis may be rejected. The null hypothesis is that the specie in question is unrepresented in the wavelength measurements. The significance parameter is calculated under the assumption of Gaussian statistics. A tolerance of 0.06 Å was used throughout.

For less securely identified species, we give a Monte Carlo estimate of the probability that the null hypothesis is correct. When this number is subtracted from unity, and multiplied by 100, we get the percentage confidence level for the identification. Thus 0.05 corresponds to the 95 per cent confidence level, which is often taken as the threshold of significance. Cowley & Hensberge (1981) give a detailed summary of the method of WCS. Current techniques are somewhat more versatile than those used at that time because *digitized* stellar intensities are available.

Significances for the most confidently identified species are shown in Table 1. Note the presence of both Fe I and II in this list. Both Ti I and II also appear as well as Co I. Interestingly, for a CP star, Cr I and II appear, at lower significances, in Table 2.

The spectra of all species that appear in Table 2 are surely present. The lower confidence levels are meaningful in some cases, such as Cr I and II, but surely not in the case of the Balmer lines, or H and K of Ca II. When the Monte Carlo estimate of the probability that the null hypothesis is correct is smaller than 0.005, we give the significance parameter. These are the numbers greater than unity. Note that while λ4215 of Sr II is surely present, it is not strong. Absorption at the position of 4077, the other line of the resonance pair of Sr II, is dominated by lanthanide lines. Sr II λ4161.80 of Mult. 3 also appears to be present.

Table 3. Additional interesting (likely and less likely) species. The column headed WCS gives the null hypothesis probability (see text for details).

Spectra	WCS	No. lines	Spectra	WCS	No. lines
C I		2	Gd I		5
O I		2	Tb I	0.045	3
Mg I		4	Dy I	0.005	14
Cu I		3	Dy III	0.015	23
Sr II		2	Ho I		8
Zr I		30	Er I	0.090	22
Nb I		2	Er III	0.035	24
Mo I		19	Tm I		3
Ru I	0.020	19	Lu I	0.020	2
Ag I		2	Ta I		10
Cd I		1	Ta II		1
In I		1	W I		44
Sn I		1	W II		3
Ba I		7	Re I		13
La I	0.035	4	Os I		8
Ce I		6	Ir I		2
Pr I		6	Th II	0.005	13
Nd I		8	Th III	0.045	15
Sm I		13	U II		10

None of the species listed in Table 3 has WCS support at better than the 99.5 per cent confidence level. The columns give the WCS result, if significant, and the number of features attributed wholly or partially to the species in question. The numbers refer to the identification lists including lines found by synthesis. Dy I and III are considered less secure than several of the entries in Table 2, even though the WCS parameters are marginally better (cf. Tb II and III).

Most of these identifications in Table 3 come from the blue–violet region.

The meaning of individual abundances derived from these species must remain uncertain. Nevertheless, the apparent presence of so many neutral lanthanide lines makes it difficult to avoid the conclusion that some of these first spectra are present, though obviously weak.

The third spectrum of thorium might be present. It is, of course, weak. We know of only one other case where the identification of the third spectrum of an actinide has been claimed for a star (cf. Cowley & Rice 1981).

No evidence was found for any oxide of a lanthanide, although several were sought. No support was found for the presence of unstable elements, technetium or promethium.

4 MODEL ATMOSPHERE CALCULATIONS

Part of the controversy surrounding HD 101065 has concerned its effective temperature. This was discussed briefly in Paper I. None of the standard-abundance Kurucz (1993) models can fit the observed colours and hydrogen line profiles. Effective temperatures in the wide range 6000–7500 K are required to fit various features. Beginning with Przybylski himself, investigators have suggested that heavy line blanketing dramatically changed the atmospheric structure of this star. Previous work clearly demonstrates abundance excesses of the rare earths and other heavy elements, and a moderate deficiency of some light and iron-peak elements. It is clear that any realistic model atmosphere for this star must take line blanketing explicitly into account.

In the temperature range relevant for the photosphere of HD 101065, about one million lines actually contribute to the total

Table 4. Comparison between the observed Strömgren and UBV indices and calculated ones using both scaled solar abundances and our HD 101065 specific ODF. $T_{\rm eff} = 6600$ K, $\log g = 3.5$ and 4.2, compositions are solar (p00) and scaled solar by +1 dex (p10) in addition to the specific ODF. $\xi_{\rm t}$ is 1 km s^{-1} for the latter, and 4 km s^{-1} (k4) for the other cases.

Index	Observations	6600g35_ODF	6600g42_ODF	6600g35_p10/p00k4	6600g42_p10/p00k4
$b-y$	0.452	0.376	0.387	0.333/0.269	0.341/0.281
m_1	0.430	0.587	0.582	0.390/0.219	0.379/0.220
c_1	−0.012	0.414	0.298	0.623/0.711	0.508/0.541
β	2.641	2.747	2.741	2.722/2.705	2.719/2.701
$B-V$	0.760	0.754	0.767	0.624/0.440	0.630/0.459
$U-B$	0.200	0.628	0.571	0.485/0.166	0.425/0.097

opacity (cf. Piskunov & Kupka 2000 for more details) for the case of a solar abundance enhanced by a factor of 10 for elements heavier than He. For solar abundance this value decreases to about 500 000. The more complex atomic structure of the REE atoms and ions explains how a greater number of spectral lines are observed in the spectrum of HD 101065. Unfortunately, atomic data for REE exist for less than 13 000 spectral lines from the neutral and first-ionization stages. For the third spectra of the REE, already becoming prominent in cool Ap stars, the necessary atomic data are only known for a small number of lines.

We have attempted to allow for the enhanced blanketing in HD 101065 in the following way. We calculated opacity distribution functions (ODFs) with the procedure described in Piskunov & Kupka (2000) using the abundances determined from observations for all but iron-peak elements. For the latter, we increased abundances by +1.5 dex to simulate missing line opacity due to lack of data for the REE. Clearly, this procedure is only approximate, because we neither know the total number of missing lines nor their real distribution with wavelength. This will in general be different from that for iron-peak elements, and this difference will affect the flux redistribution. We used iron-peak overabundances only in ODF calculations to obtain the T–τ relation. The equation of hydrostatic equilibrium was then integrated using our best estimates of the actual abundances to determine the opacity.

Our adopted ODF is thus a first approximation to the real opacities in the photosphere of HD 101065. For comparison and to determine preliminary abundances we used the ODFs of Kurucz (1992, 1993) with abundances for elements heavier than He scaled by +1 dex and a (pseudo-) microturbulence velocity $\xi_{\rm t}$ of 4 km s^{-1} to account for missing opacity and for magnetic broadening. We also tried ODFs based on $\xi_{\rm t} = 1$ km s^{-1} (magnetic broadening only), and ODFs representing the same range of $\xi_{\rm t}$, but with solar chemical composition (cf. Kurucz 1992 for details).

The model atmosphere calculations were performed with modifications of the ATLAS9 code of Kurucz (1992, 1993). The modifications concerned both the input procedures for our own ODF (cf. Piskunov & Kupka 2000) as well as the convection model employed.

One might expect convection to be be more important in this star than for other roAps, because of the lower temperature and increased opacity. But our calculations show that the enhanced opacity leads to such a lowering of the gas pressure for relevant optical depths that convection is of little significance. The heat capacity per unit volume is simply too low. Similar results have been found for any convection model recently implemented into ATLAS9 (a summary of the latter is given in Kupka 1996 and in Gardiner, Kupka & Smalley 1999). The same observation is readily made when comparing model atmosphere grids with different metallicity calculated by Kurucz (1992), among others.

For our analysis of HD 101065 spectra, we have chosen the convection model due to Canuto & Mazzitelli (CM, 1991) implemented into ATLAS9 by Kupka (1996); it predicts the lowest convective efficiency for our parameters for HD 101065 among all convection models available for the ATLAS9 code.

Earlier in 1999, heavily blanketed models for Przybylski's star based on the opacity sampling technique were calculated at our (CRC's) request by R. L. Kurucz with ATLAS12, and Bengt Edvardsson, using codes available at Uppsala. The basic T–τ relations from both sets of calculations resemble our adopted model. In particular, both agree that convection is virtually absent. Some additional details are given by Cowley (1999) (see also http://www.aas.org/publications/baas/v31n5/aas195/-Author Index.htm#C). We thank both colleagues for their help.

The observed Strömgren and UBV colours are given in Table 4 along with calculations for model atmospheres based on our individual ODF and models with solar abundances scaled upward. The observed values are from the SIMBAD data base. Colour indices are calculated for $\log g = 3.5$ and 4.2 with the procedure generally described by Relyea & Kurucz (1978), as applied in Smalley & Kupka (1997). Note the calculated colours include only lines with known atomic parameters, and are provisional. Nevertheless, on the basis of overall differences of observed and calculated colours, the $\log g$ 4.2-ODF model is the best. The latter $\log g$ is more typical for roAp stars (see Ryabchikova et al. 1999). Models based on our ODF with individual abundances fit the observed indices better, in particular the unusually low c_1 index. The remaining discrepancies obviously require further improvements of the model atmosphere in order to be resolved. Fig. 1 shows that the T–τ relation due to the HD 101065-specific ODF cannot be mimicked by simple scaling of the solar metallicity. Further discussion on the structure of this model atmosphere can be found in Piskunov & Kupka (2000).

For the final abundance analysis, we accepted the following ODF model: $T_{\rm eff} = 6600$ K, $\log g = 4.2$, $\xi_{\rm t} = 1$ km s^{-1}.

5 MAGNETIC FIELD AND ROTATION

When we compared observed and synthetic spectra we found a few lines of Sm II and Gd II with effective Landé factors close to 2.0, which show partially resolved splitting. To check the possibility that this splitting is due to the Zeeman effect we calculated synthetic spectra in the region of three lines: Gd II λ5749.39 ($g_{\rm eff} = 2.09$), Sm II λ6294.68 ($g_{\rm eff} = 1.97$) and Gd II λ6610.06 ($g_{\rm eff} = 1.65$), taking into account the magnetic field. We used the SYNTHMAG code (Piskunov 1999). This code was

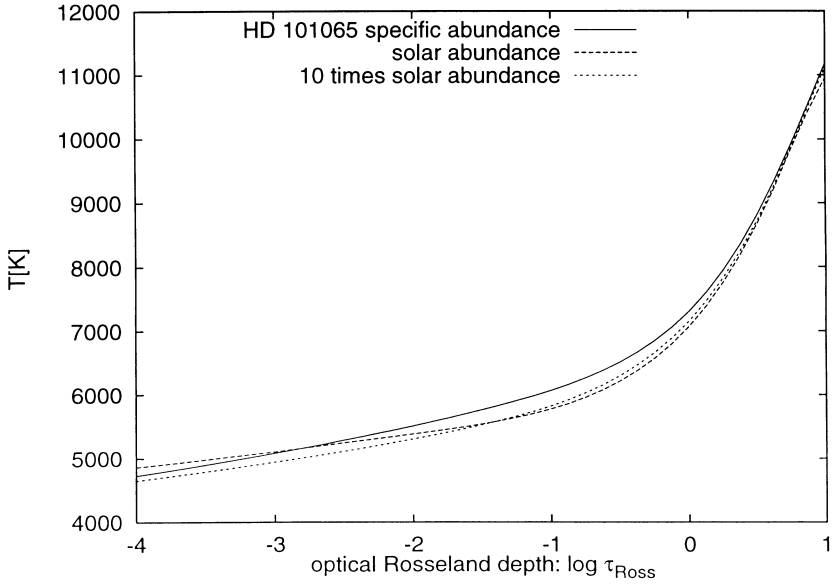

Figure 1. T–τ relation for $T_{\rm eff} = 6600$ K, $\log g = 3.5$, $\xi_{\rm t} = 1\,{\rm km\,s^{-1}}$ and different chemical compositions.

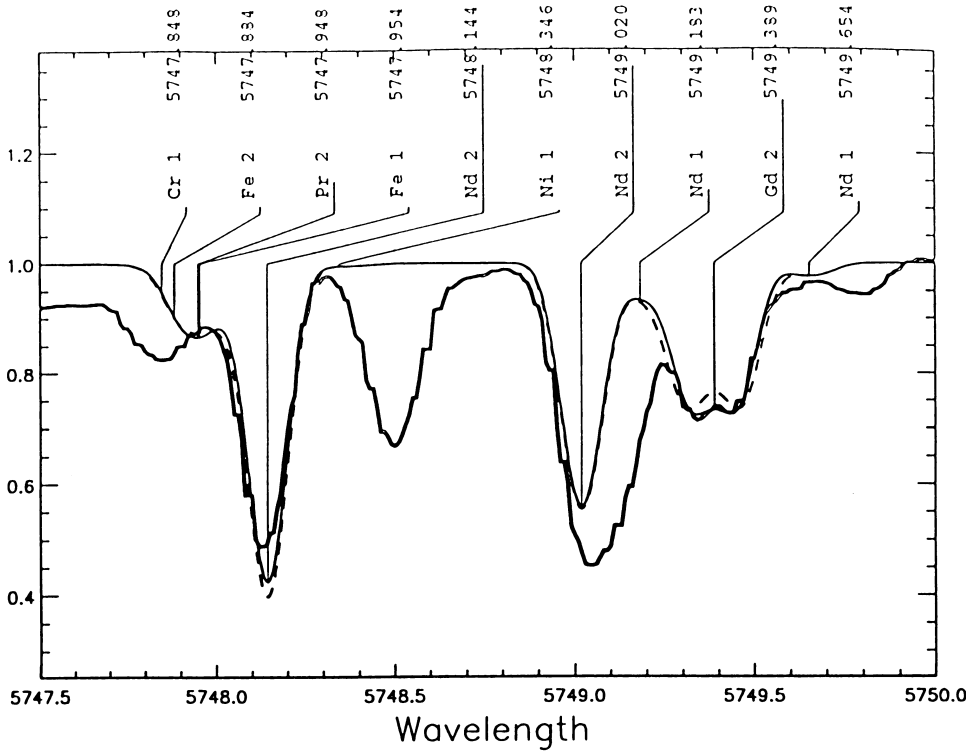

Figure 2. A comparison between observed (tube line) and synthesized with $B_{\rm s} = 2300$ G (solid line) and with $B_{\rm s} = 2650$ G (dashed line) spectrum near the Gd II λ5749.39 line.

successfully applied to the magnetic synthesis of Eu lines in a sample of cool Ap stars (Ryabchikova et al. 1999). Observed line profiles of HD 101065 may be well represented by synthetic profiles calculated with a mean surface magnetic field (magnetic modulus) $B_{\rm s} = 2300 \pm 350$ G. Fig. 2 shows a comparison between the observed and calculated spectrum near the Gd II λ5749.39 line. The derived value of the magnetic modulus agrees with the longitudinal field, -1408 G obtained in Paper I, and is also consistent with the values -2100 to 2500 G reported by Wolff & Hagen (1976).

Magnetic synthetic calculations also allow more accurate estimates of stellar rotational velocity. The final value $v \sin i = 3.5 \pm 0.5\,{\rm km\,s^{-1}}$ was obtained in comparison with a minimal value $v \sin i = 5\,{\rm km\,s^{-1}}$ measured with non-magnetic synthetic calculations. In the spectrum of a magnetic star, each line has its own width, so one never measures a unique rotational velocity. This is also easily seen in Fig. 2. The width of two lines Nd II λ5748.144 ($g_{\rm eff} = 0.03$) and Gd II λ5749.389 ($g_{\rm eff} = 2.09$) is different. If we fit both lines with a simple synthetic spectrum neglecting magnetic broadening, we have to convolve the first line

Table 5. Abundances calculated with WIDTH9 for microturbulences 1 and 2 km s^{-1}, and with SYNTHMAG code for $B_s = 2.3$ kG with zero microturbulence. For Co I lines hyperfine structure was taken into account in magnetic synthesis.

Species	Wavelength (Å)	Equivalent width (mÅ)	$g_{\rm eff}$	Abundance ($\log(N/N_{\rm tot})$ $\xi_t = 1$ km s^{-1}	$\xi_t = 2$ km s^{-1}	SYNTHMAG
Fe I	5238.039	72	1.13	−6.00	−6.30	−6.05
Fe I	5365.399	20	0.95	−5.36	−5.39	−5.32
Fe I	5393.168	50	1.50	−5.27	−5.41	−5.32
Fe I	5405.775	52	0.75	−5.99	−6.14	−5.99
Co I	6082.422	42	1.33	−5.57	−5.69	−5.80(hfs)
Co I	6188.996	22	1.48	−5.59	−5.63	−5.60(hfs)
Ce II	5393.392	82	1.01	−7.53	−8.17	−7.45
Pr II	6087.533	63	1.00	−8.18	−8.55	−8.30
Nd II	5399.099	79	−0.10	−6.93	−7.55	−7.40
Nd II	5748.144	90	0.03	−6.93	−7.64	−7.48
Sm II	6174.944	66	1.87	−7.40	−7.82	−7.80
Sm II	6181.048	65	1.49	−7.40	−7.80	−7.60
Gd II	5749.389	73	2.09	−6.90	−7.46	−7.50
Gd II	6080.641	109	1.10	−6.24	−7.09	−7.10
Gd II	6180.428	65	0.96	−7.32	−7.74	−7.70
Gd II	6610.035	34	1.65	−7.33	−7.45	−7.45

with $v \sin i = 5$ km s^{-1}, while for the second line a value $v \sin i \approx 8$ km s^{-1} is required.

6 MICROTURBULENCE AND MAGNETIC BROADENING

In principle, the abundance analysis of a star with a magnetic field has to be done with the magnetic field taken into account in spectral synthesis. But the model atmosphere uncertainties and a rather small value of the magnetic field allow a simplified analysis. With a few exceptions we used the Kurucz (1993) WIDTH9 code modified by V. Tsymbal (see Ryabchikova et al. 1997b). For the most important partially blended lines, we performed magnetic synthetic calculations. Atomic parameters needed for abundance calculations have been extracted from the latest revision of VALD–2 (Kupka et al. 1999). Detailed references will be given below.

Microturbulence was estimated from iron lines in the usual way by removing any dependence of the equivalent widths on the individual line abundances. From iron lines we got a value of $\xi_t \approx 1$ km s^{-1}. Test magnetic synthetic calculations of a few Fe I lines with different magnetic field values show that the magnetic intensification effect might be roughly approximated with a magnetic pseudo-microturbulence by the following relation: $\xi_t(\text{km s}^{-1}) = 0.41 \times B(\text{kG})$. Our estimated value of the magnetic field, 2.3 kG produced a pseudo-microturbulence close to 1 km s^{-1}. This means that the microturbulence in the atmosphere of HD 101065 could be *totally* due to the magnetic field. In this case it should be different for atomic species with different average magnetic splitting and with different line intensities. In fact, for REEs the usual procedure of the microturbulence determination leads to a higher value of ξ_t, close to 2 km s^{-1}. To illustrate the magnetic intensification effect we compared abundances calculated for a few chosen Fe I, Co I and REE lines using magnetic spectrum synthesis with zero microturbulence, and the WIDTH9 code with different microturbulence values. The results are presented in Table 5. For Co I lines we also included hyperfine structure in magnetic synthesis. Hyperfine structure constants were taken from Biehl (1976). The combined hyperfine structure and magnetic effects result in higher value of the pseudo-microturbulence obtained in usual abundance analysis even for lines of moderate intensity.

7 ABUNDANCE ANALYSIS

Calculations were carried out in Michigan in parallel with those in Moscow and Vienna, using the suite of programs described in Paper I. In the equivalent width mode, the Michigan code SYNTH2 matches the Moscow–Vienna results to within 0.05 or better if the same equivalent widths are used. The automatic synthesis code MERSEN gives results within 0.2 dex of the other results. For a 111-line set, with W_λ ranging from 5 to 144 mÅ, the *average* difference in the equivalent width measurements was only 1 per cent. The average absolute value of the percentage differences was 15 per cent.

Table 6 gives a summary of the abundances of 54 elements in the atmosphere of HD 101065, obtained (or estimated) for microturbulences of 1 and 2 km s^{-1}. For comparison, we present abundances for two other very cool roAp stars: HD 122970 (Ryabchikova et al. 2000a), and HD 24712 (Ryabchikova et al. 1997b). The column headed 'Sun' contains abundances based on Grevesse & Sauval's (1998) table 1. Most of the entries are from their column 3 (Meteorites). Missing entries are supplied from their column 2. Abundances estimated from one line are considered as uncertain; they are marked by ':'.

In Fig. 3 the abundances are shown plotted against the atomic number Z. They will be discussed in the sections below.

7.1 Light elements: C to S

Oscillator strengths for C and O were taken from the recent NIST compilation (Wiese, Fuhr & Deters 1996), which is also available through VALD–2. Both elements are slightly deficient in HD 101065, as for many other cool Ap stars. Na, Si and S are nearly solar, but the derived abundances strongly depend on the sample of spectral lines used. Resonance Na I lines are weakened and correspond to −1.5 dex sodium deficiency in comparison with the abundance in Table 6 obtained by using lines of multiplets 4 and 5. The latter lines, in particular λλ5682.6, 5688.2, are wide and have flat cores. Also Si II lines λλ6347.1 and 6371.4 of the

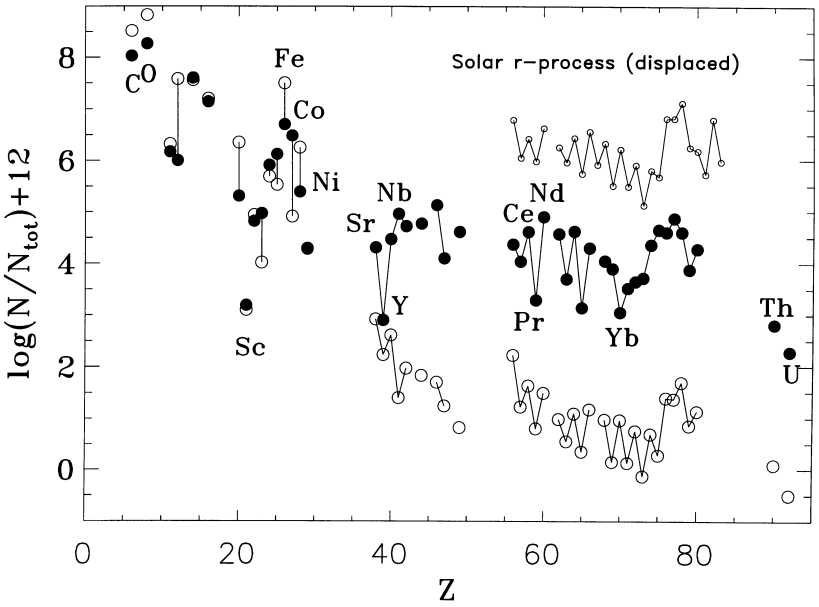

Figure 3. Calculated abundances versus Z. Filled circles are for HD 101065. Open big circles are solar abundances from Grevesse & Sauval (1998). Solar r-process abundances from Käppeler, Beer & Wisshak (1989) are plotted above for the heavy elements by small open circles. Their distribution has been displaced upward. A point has not been plotted for Ho (Z = 67) because we have used only a single Ho I line, and the first spectra of the lanthanides are generally discordant (see discussion in text).

multiplet 2 are wider and more shallow than lines of the multiplets 4 and 5. It is not possible to fit any of those lines with the spectral synthesis.

All magnesium lines are heavily blended, and synthetic spectrum calculations in the region of Mg II λ4481 and the Mg I $\lambda\lambda$5167-72-83 triplet allow only an abundance estimate for this element. It looks as though magnesium is strongly underabundant, which is also observed in another cool roAp star, HD 24712, in the phase of magnetic field and REE maximum.

7.2 Iron group (3d) elements: Ca to Ni

Abundances of most of the elements of this group vary from about an order of magnitude below solar (Ca, Fe, Ni), to normal solar abundances (Sc, Ti, Cr and Mn) to an overabundance of V and Co. A cobalt overabundance of ~1.0–1.5 dex seems to be typical for all roAp stars studied until now (see table 4 in Ryabchikova et al. 1997b). Our calculations show that this result does not change after taking into account hyperfine structure. The Ca and Fe abundances obtained in the present study agree with the results from Paper I. Iron deficiency is also observed in HD 24712, while this element is nearly solar in HD 122970.

We note a tendency for Fe I lines with low excitation potential to show lower abundances than lines with higher excitation potential. This may be connected with both the adopted atmospheric structure and with a possible abundance stratification.

7.3 Fourth and fifth period elements: Cu to Sn, and Ba

In most Ap star abundance determinations, only Sr, Y, Zr and Ba are considered. Rather scarce data exist for a few other elements: Cu and Zn in HD 203932 (Gelbmann et al. 1997), Nb and Mo in γ Equ (Ryabchikova et al. 1997a) and In in HD 24712 (Ryabchikova et al. 1997b). Cu is normal and Zn is deficient in HD 101065, and a similar behaviour is observed for two other roAp stars, HD 203932 and HD 122970.

A large difference in abundances obtained from Y I and Y II lines might be explained by an unknown blend at the position of the only Y I line that was measured. All other lines are in blends, but still their intensity in the synthetic calculations does not contradict the high yttrium abundance derived from the Y I λ5527.5 line. A smaller difference is obtained for γ Equ and for HD 122970.

For HD 101065, we could derive or estimate abundances for 11 out of 18 elements of the fifth period. For Ru I, recent oscillator strength measurements by Wickliffe, Salih & Lawler (1994) were used. Silver abundance was estimated by synthesis of the two strongest lines in the $\lambda\lambda$4000–6620 spectral region, Ag I $\lambda\lambda$5209.1 and 5465.5, both of which are in the wings of strong lines. They provide consistent abundances within 0.2 dex. Rb I lines are all in heavy blends, so it is not possible to make any reasonable estimate of its abundance. Although all Rh I lines are in heavy blends, too, synthetic spectrum calculations for the whole spectral region $\lambda\lambda$4500–6620 show that the same overabundance of Rh as observed for the adjacent elements would not produce any spectral feature stronger than the observed spectrum. Therefore, we may conclude that all elements of the fifth period are overabundant by 1.5–3.0 dex, as derived from the lines of the neutral atoms. The same conclusion is valid for barium. Note also that for some elements the derived abundances are upper limits only, and the given standard deviations are more or less formal and do not represent the real dispersion. For example, two lines of Nb I provide a consistent abundance. When we recalculate the spectrum for the whole observed region with this abundance and compare it with observations, we see that some other Nb I features in the synthetic spectrum are much stronger than the observed ones. This means that our Nb abundance may be overestimated.

The situation changes when we deal with the lines of singly ionized Sr, Y and Ba. Resonance Sr II and Ba II lines as well as

Table 6. Abundances of the roAp star HD 101065 with error estimates based on n measured lines. The abundances for two other very cool roAp stars, HD 122970 and HD 24712 (phase of magnetic and REE maximum), are given for comparison.

Ion	HD 101065 $\log(N/N_{\rm tot})$		n	HD 122970	HD 24712(max B_ℓ)	Sun
	$\xi_{\rm t}=1\,{\rm km\,s^{-1}}$	$\xi_{\rm t}=2\,{\rm km\,s^{-1}}$		$\log(N/N_{\rm tot})$	$\log(N/N_{\rm tot})$	$\log(N/N_{\rm tot})$
C I	−3.97±0.01	−3.98±0.01	2	−3.51		−3.52
O I	−3.72±0.25	−3.74±0.25	2	−3.35		−3.21
Na I	−5.81±0.23	−5.86±0.22	4	−5.87		−5.72
Mg I	∼−6.00		synth	−4.50	−5.60	−4.46
Si I	−4.38±0.24	−4.42±0.26	7	−4.45		−4.48
Si II	−4.43±0.37	−4.47±0.37	3	−4.24	−4.43	−4.48
S I	−4.86:	−4.86:	1	−4.83		−4.84
Ca I	−6.67±0.34	−6.72±0.36	5	−5.45	−5.69	−5.69
Sc II	−8.79±0.53	−8.84±0.51	6	−8.66		−8.94
Ti I	−7.08±0.29	−7.14±0.29	5	−6.91	−7.29	−7.10
Ti II	−7.18±0.29	−7.33±0.27	11	−6.86	−7.28	−7.10
V I	−6.85±0.38	−6.90±0.36	7	−7.84		−8.02
V II	−7.16±0.29	−7.20±0.28	6	−7.73		−8.02
Cr I	−6.19±0.21	−6.24±0.25	9	−5.99	−5.80	−6.35
Cr II	−5.92±0.26	−6.00±0.27	15	−5.94	−5.33:	−6.35
Mn I	−6.04±0.27	−6.23±0.32	8	−6.40	−7.01	−6.51
Mn II	−5.62±0.04	−5.64±0.05	2	−6.31		−6.51
Fe I	−5.41±0.26	−5.51±0.30	35	−4.48	−4.88	−4.54
Fe II	−5.10±0.22	−5.17±0.23	9	−4.44	−5.11	−4.54
Co I	−5.67±0.20	−5.76±0.22	32	−6.06	−5.57	−7.13
Co II	−5.32:	−5.34:	1	−5.84	−5.53	−7.13
Ni I	−6.58±0.34	−6.65±0.31	5	−5.89	−6.34	−5.79
Cu I	−7.68±0.07	−7.77±0.04	2	−8.13		−7.75
Zn I	⩽−8.35	⩽−8.44	2	−7.80		−7.37
Sr I	−7.31:	−7.36:	1			−9.12
Sr II	−7.74±0.04	−8.34±0.06	2	−7.31	−8.20	−9.12
Y I	−7.67:	−7.72:	1	−8.67	−7.80	−9.81
Y II	−8.99±0.24	−9.22±0.31	7	−9.09	−8.30	−9.81
Zr I	−7.50±0.46	−7.62±0.44	3	−8.41		−9.43
Zr II	−7.39±0.20	−7.61±0.14	11	−8.48		−9.43
Nb I	−7.00±0.04	−7.08±0.06	2			−10.64
Mo I	−7.21±0.26	−7.36±0.30	5			−10.07
Ru I	−7.21±0.33	−7.25±0.32	3			−10.21
Pd I	−6.84±0.11	−6.91±0.13	4			−10.34
Ag I	−7.90:		synth			−10.80
Cd I	⩽−7.70		1			−10.28
In I	−7.02:	−7.76:	1		−9.00	−11.22
Sn II	⩽−7.60		1			−9.90
Ba I	−7.32±0.24	−7.37±0.22	6	−8.13		−9.82
Ba II	−7.69±0.01	−8.15±0.30	2	−8.99	−8.98	−9.82
La II	−7.75±0.35	−8.17±0.29	28	−9.34	−8.75	−10.82
Ce II	−7.19±0.33	−7.60±0.26	46	−8.82	−8.90	−10.41
Pr I	−6.27±0.23	−6.40±0.21	4			−11.24
Pr II	−8.63±0.31	−8.80±0.21	31	−10.04	−9.60	−11.24
Pr III	−7.05±0.36	−7.46±0.16	12	−8.63		−11.24
Nd I	−6.34±0.39	−6.39±0.35	6			−10.55
Nd II	−6.91±0.34	−7.65±0.28	71	−9.23	−8.64	−10.55
Nd III	−6.52±0.40	−7.31±0.30	7	−8.39		−10.55
Sm II	−7.12±0.39	−7.75±0.29	41	−9.33	−9.16	−11.06
Eu II	−8.03±0.41	−8.58±0.19	5	−9.66	−9.00	−11.49
Gd II	−7.14±0.38	−7.62±0.25	35	−8.69	−8.70	−10.95
Tb II	−8.83±0.17	−8.89±0.16	3	−10.00		−11.69
Dy II	−7.52±0.27	−7.88±0.23	16	−9.07	−8.94	−10.87
Ho I	−6.59:	−6.60:	1			−11.53
Er II	−7.82±0.28	−8.09±0.22	18	−9.63	−9.53	−11.07
Er III	−6.51±0.28	−6.83±0.04	4	−7.60		−11.07
Tm II	−8.00±0.28	−8.20±0.28	15	−9.04		−11.89
Yb II	−8.92±0.34	−8.99±0.33	9	−9.83		−11.08
Lu II	−8.31±0.28	−8.65±0.14	6	−9.75		−11.91
Hf II	−8.28±0.25	−8.42±0.21	3	−8.66		−11.29
Ta I	−8.19±0.42	−8.22±0.39	3			−12.17
Ta II	−8.19:	−8.51:	1			−12.17
W I	−7.45±0.49	−7.58±0.41	4			−11.35
W II	−7.67±0.26	−7.84±0.18	3			−11.35
Re I	−7.32±0.02	−7.39±0.02	2			−11.76
Os I	−7.40±0.30		synth			−10.65
Ir I	−7.11±0.07	−7.16±0.07	2			−10.67

Table 6 – *continued*

Ion	HD 101065 $\log(N/N_{\rm tot})$ $\xi_{\rm t}=1\,{\rm km\,s^{-1}}$	HD 101065 $\log(N/N_{\rm tot})$ $\xi_{\rm t}=2\,{\rm km\,s^{-1}}$	n	HD 122970 $\log(N/N_{\rm tot})$	HD 24712(max B_ℓ) $\log(N/N_{\rm tot})$	Sun $\log(N/N_{\rm tot})$
Pt I	−7.37±0.25	−7.44±0.24	4			−10.35
Au I	−8.11:	−8.13:	1			−11.19
Hg I	−7.66±0.12	−7.78±0.08	2			−10.91
Th II	−9.17±0.18	−9.22±0.17	13			−11.95
U II	−9.70:	−9.74:	1			−12.54
$T_{\rm eff}$	6600			6930	7250	
$\log g$	4.20			4.11	4.30	
B_s (kG)	2.3			2.2	3.0	

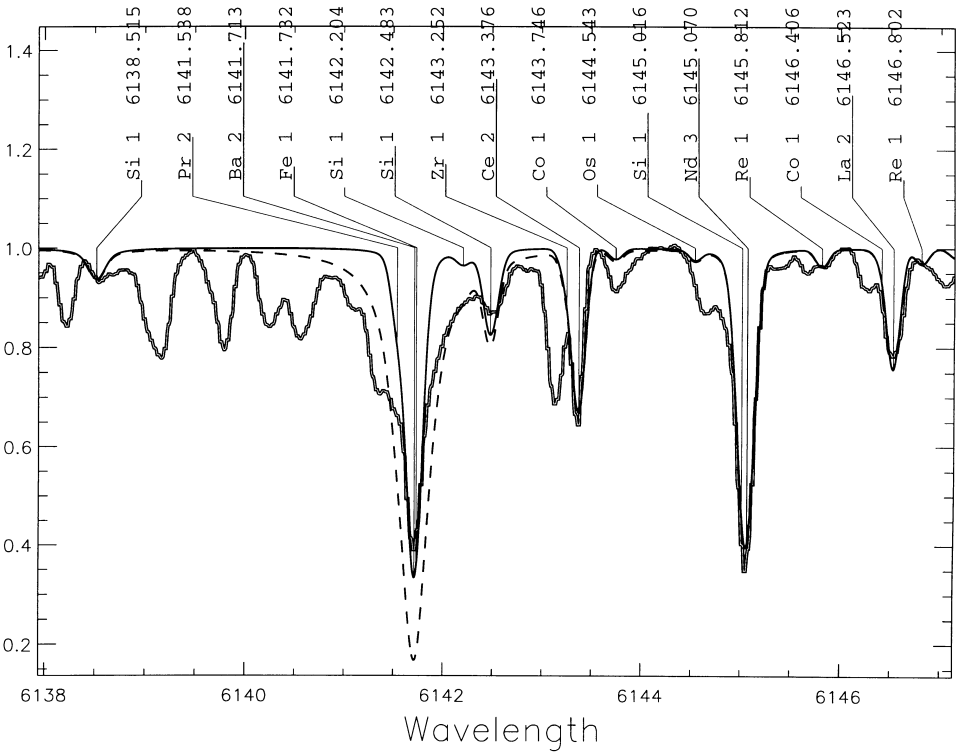

Figure 4. A comparison between observed (tube line) and synthesized with $\log(N/N_{\rm tot})=-8.8$ (solid line) and with $\log(N/N_{\rm tot})=-7.6$ (dashed line) spectrum near the Ba II λ6141.7 line.

strong Ba II lines of multiplet 2 have unusually strong wings and cores that are narrow and not deep. Line profiles cannot be fitted with a single abundance. The barium abundance from Ba II lines in Table 6 was obtained using integrated equivalent widths. If we try to fit a line core we get an abundance about an order of magnitude smaller than derived from the equivalent width. Fig. 4 shows a comparison between the observed and calculated line profiles for Ba II λ6141.7. Calculations were made for the following barium abundances: close to that obtained from Ba I lines (−7.6) and as obtained from the best fit of the line core (−8.8).

For the Ca K line, the same peculiarity was explained by Babel (1992) in the frame of a diffusion model with a weak stellar wind. He predicted an inhomogeneous distribution of Ca, Fe, Mn and Cr with a higher element concentration in the deeper layers. The difference between concentrations at $\log\tau_{5000}=0$ and $\log\tau_{5000}=-2$ may exceed 2.0 dex. However, it is difficult to produce such a stratification for heavier elements like Sr, Ba, La and other REEs, for which radiative acceleration exceeds gravity through the whole atmosphere and becomes smaller only in the deep layers with $\log\tau_{5000}>0.8$. Babel mentioned that abundance stratification depends strongly on the exact locus and extension of the hydrogen convection zone. If the bottom of the convection zone is situated where gravity exceeds radiative acceleration and the diffusion velocity is negative, then after a short time an element will be underabundant in the reservoir, and hence in the atmosphere. Babel mentioned that a corona may also play a positive role in creating strong overabundances of heavy elements. Qualitatively, a diffusion model with a weak wind may explain many of the observed abundance anomalies in HD 101065, while real diffusion calculations are needed to make a self-consistent model of the abundance distribution in the atmosphere of this star.

7.4 Rare-earth elements

7.4.1 New oscillator strengths

New *gf*-values for Nd III and Pr III were calculated using the

Cowan code (Cowan 1981, 1985) as part of this study. A full account of the methodology, results and assessment of the data on Nd III has been given by Bord (2000). Part of the Nd III data were published by Cowley & Bord (1997). Briefly, log(*gf*) values for over 9000 lines of Nd III in the range $\lambda\lambda$3000–6000 and for more than 1000 lines of Pr III in the interval $\lambda\lambda$2000–8000 were computed. Comparisons of published experimental data with previous Cowan-code calculations of this type for other lanthanide rare-earth ions (viz. La II Bord, Barisciano & Cowley 1996; Ce III Bord, Cowley & Mirijanian 1998; and Lu II Bord, Cowley & Norquist 1997) suggest that, for transitions with cancellation factors (cf. Cowan 1981, equation 14.107) substantially greater than 0.1 in absolute value and *in the absence of significant core polarisation effects*, the uncertainty in the log(*gf*) values is about $\pm$0.15 dex. Since the aforementioned conditions generally apply to the strong lines of Nd III and Pr III used in our analysis of HD 101065, we expect that the uncertainties in the log(*gf*) values will set a lower limit on the accuracy of our abundances for Nd and Pr derived from these ions; residual uncertainties associated with our choices of model atmosphere and broadening parameters for this star, the use of predominantly saturated lines on the flat part of the curve of growth, line blending (and the wavelength shifts often occasioned by such blending) which, in extreme cases, poses challenges for our synthesis routines, and other systematic effects can easily raise the total error by another 0.1–0.2 dex for these species. For Er III, oscillator strengths were recently calculated by Wyart et al. (1997).

We also used recent experimental measurements of the oscillator strengths for Tm II (Wickliffe & Lawler 1997).

7.4.2 Abundances

The REE abundances listed in Table 6 supersede those published in Paper I. The latter are in error by roughly one order of magnitude due to the use of a corrupted file by CRC.

It is now possible to obtain abundances from three ionization stages for Pr and Nd.

All neutral species for which we have measured line equivalent widths give higher average abundances than first and even second ions. The reason may be the same as in the case of Nb discussed in Section 7.3: nice lines suitable for measurements are not the main contributors to the observed feature, which may belong to some unknown line of the first or second REE ions. Our synthetic spectrum calculations for the whole spectral region with REE abundances from the first ions show that some lines of the neutral REE correspond to these abundances and do not require higher abundances. For example, Gd I λ6114.04 fits the observed spectrum with Gd abundance $-$7.35; a blend of three lines Gd I λ4683.337, Zr I λ4683.438 and Nd I λ4683.663 fits nicely the observed feature with the abundances from Table 6 corresponding to the first ions; there are no observed features at the positions of Nd I $\lambda\lambda$4891.054, 4924.521, 4944.826, while even with the Nd abundance extracted from the first ions, weak features are produced in the synthetic spectrum.

We believe it is premature to draw any conclusions based on lines of neutral REEs at this time.

For three REEs, Pr, Nd and Er, we were able to derive abundances from the second ions. They exceed those obtained from the first ions of the same element by 1.6, 0.4 and 1.3 dex, respectively. For Nd, we can still claim that the abundances obtained from all three ionization stages are roughly similar, while for Pr and Er the difference is large and cannot be explained by oscillator strength uncertainties or by the neglect of hyperfine structure and/or isotopic shifts. Even larger differences were found in HD 122970 (see Table 6), and this seems to be a characteristic feature of roAp stars, while no ionization discrepancy is observed for a few cool non-roAp stars (Ryabchikova et al. 2000b). A simple stratification model proposed by Babel (1992) (see the discussion in Section 7.3) cannot provide a reasonable fit for both Pr species with a unique abundance distribution. The same has been checked for the opposite case where the concentration of the element is increased in the upper atmospheric layers.

7.5 Heavy elements

We tried to obtain or estimate abundances for all stable elements heavier than Lu for which atomic data are available in VALD–2. Owing to the limited number of spectral lines and blending problems in the HD 101065 spectrum, we consider our abundances to be upper limits. An encouraging fact is that in two cases when we observed spectral lines from two ions (Ta, W) we obtained consistent abundances. A fit for the Re I λ 6145.9 line is shown on Fig. 4. Most abundances follow the odd–even rule and, remarkably, repeat the solar-system abundance pattern.

8 CONCLUSIONS

8.1 The model

Our current atmospheric model can only be regarded as a first approximation because of missing atomic data and thus an incomplete account of opacity. Although the artificial enhancement of iron-peak elements in comparison with the derived element abundances has brought synthetic photometric colours closer to the observed ones, some discrepancies still remain. Also, from spectroscopy we found several indications that the model atmosphere still has to be improved, in particular from a comparison of abundances derived from lines of different ionization stages of a given element. The origin of these differences, however, may be at least partially explained by the heavy line blending and still missing line identifications. The next step in modelling the photosphere of HD 101065 must once more be to extend the basis for realistic opacity calculations. Suitable data for the second ionization stage of REEs are still scarce and data on neutral atoms and first ions of the REEs are still fairly incomplete. In addition to improved atomic data, model atmospheres taking vertical stratification into account may be necessary to explain the remaining differences between model predictions and observations.

8.2 The abundances

Generally speaking, the abundances plotted in Fig. 3 show the pattern of other CP stars, and may be accounted for within the theory proposed by Michaud (1970). Elements with high abundances in the standard abundance distribution (SAD) (cf. e.g. Grevesse & Sauval 1998) show depletions; those with low abundances show enhancements. Radiation pressure, primarily due to absorption lines, will support an atom or ion until saturation sets in, when the flux in the lines decreases rapidly. We thus expect a rough maximum for all elemental abundances. Individual elements may fail to reach this plateau, for example, when the noble gas structure is relevant.

A close examination of Fig. 3 leads to a number of questions

not easily answered within the above context. First, why do only the light elements scatter in their departure from solar abundances? If we take an average of the first 16 elements, the average departure from solar is only 0.1 dex. The largest departure is for cobalt, which is enhanced by 1.6 dex. Scandium, on the other hand, which has the lowest solar abundance among the light elements determined here, is neither enhanced nor depleted.

While the lighter elements scatter about a SAD mean, the heavier elements show an overall enhancement of some 3 dex. The coherence of the abundances is remarkable. With a few exceptions, the entire solar distribution appears to be displaced uniformly upward. There is even a shadow of the third r-process peak, though displaced toward lower Z.

There is a significant departure from the odd–even effect at Yb ($Z = 70$), which is less abundant than its odd-Z neighbours. The determination is based on nine lines, and should not be markedly less reliable than those of its congeners. Note that the abundances for elements on the 'quasi-r-process peak' are primarily from first spectra, while those plotted for the lanthanides are from second spectra. This raises the possibility that the feature is spurious, and should be examined more closely. One element within the feature, W ($Z = 74$), has abundances in fair agreement from several lines of both first and second spectra.

Departures from a displaced SAD pattern may provide the key to understanding how it is possible that so many elements are enhanced by such large factors while preserving their overall relation to one another.

ACKNOWLEDGMENTS

This paper is based on observations collected at the European Southern Observatory (La Silla, Chile), within the framework of programme 60.E-0563. CRC thanks R. L. Kurucz and B. Edvardsson for their calculations of line-blanketed models, as well as D. Mihalas and H. Holweger for comments on heavily blanketed models. TR thanks her collaborator, E. S. Davydova, for help in measuring the HD 101065 spectrum. FK and TR thank the Austrian Fonds zur Förderung der wissenschaftlichen Forschung (FwF project S7303-AST) for financial support. Part of FK's work on HD 101065 has been funded through FwF project P11882-PHY. TR thanks the Russian Fund for Basic Research (Grant 98-02-16734) for financial support. We gratefully acknowledge the use of the SIMBAD data base.

REFERENCES

Babel J., 1992, A&A, 258, 449
Bidelman W. P., Cowley C. R., Iler A. L., 1995, Pub. Obs. U. Mich., 12, 77
Biehl D., 1976, PhD thesis, Christian-Albrechts-Universität, Institüt für Physik und Sternwarte, p. 187
Bord D. J., 2000, A&AS, in press
Bord D. J., Desko R. D., 1986, in New Insights in Astrophysics: Eight Years of UV Astronomy with IUE, ESA SP-263, p. 409
Bord D. J., Barisciano L. P. Jr, Cowley C. R., 1996, MNRAS, 278, 997
Bord D. J., Cowley C. R., Norquist P. L., 1997, MNRAS, 284, 869
Bord D. J., Cowley C. R., Mirijanian D., 1998, Solar Phys., 178, 221
Canuto V. M., Mazzitelli I., 1991, ApJ, 370, 295
Conway J. G., Worden E. F., 1970, Preliminary analysis of the first and second spectra of dysprosium, Dy I and Dy II. Lawrence Radiation Laboratory, UCRL-19944
Corliss C. H., 1973, J. Res. (US) Nat. Bur. Stds, 77A, 419
Cowan R. D., 1981, The Theory of Atomic Structure and Spectra. Univ. California Press, Berkeley
Cowan R. D., 1985, Programs RCN/RCN2/RCG/RCE, Los Alamos Natl Lab.
Cowley C. R., 1999, Bull. AAS., 31, 1447
Cowley C. R., Bord D. J., 1997, in Brandt J. C., Ake T. B., Petersen C. C., eds, ASP Conf. Ser., 143, The Scientific Impact of the Goddard High Resolution Spectrograph. p. 346
Cowley C. R., Hensberge H., 1981, ApJ, 244, 252
Cowley C. R., Mathys G., 1998, A&A, 339, 165 (Paper I)
Cowley C. R., Rice J. B., 1981, Nat, 294, 636
Gardiner R. B., Kupka F., Smalley B., 1999, A&A, 347, 876
Gelbmann M., Kupka F., Weiss W. W., Mathys G., 1997, A&A, 319, 630
Grevesse N., Sauval A. J., 1998, Space Sci. Rev., 85, 161
Hack M., 1976, in Weiss W. W., Jenkner H., Wood H. J., eds, IAU Colloquium 32, Physics of Ap Stars. Universitätssternwarte, Vienna, p. 255
Käppeler F., Beer H., Wisshak K., 1989, Rep. Prog. Phys., 52, 945
King A. S., 1943, ApJ, 97, 323
Kupka F., 1996, in Adelman S. J., Kupka F., Weiss W. W., eds, ASP Conf. Ser. 108, Model Atmospheres and Spectrum Synthesis. p. 73
Kupka F., Piskunov N., Ryabchikova T. A., Stempels H. C., Weiss W. W., 1999, A&AS, 138, 119
Kurtz D. W., 1990, ARA&A, 28, 607
Kurucz R. L., 1992, in Barbuy B., Renzini A., eds, The Stellar Populations of Galaxies, IAU Symp. 149. Kluwer, Dordrecht, p. 225
Kurucz R. L., 1993, SAO, Cambridge, Kurucz CDROM 2, CDROM 13
Mathys G., Hubrig S., 1997, A&AS, 124, 475
Meggers W. F., Corliss C. H., Scribner B. F., 1975, NBS Monog. No. 145 (Monograph 145)
Michaud G., 1970, ApJ, 160, 641
Piskunov N. E., 1992, in Glagolevskij Yu.V., Romanyuk I. I., eds, Stellar Magnetism. Nauka, St Petersburg, p. 92
Piskunov N. E., 1999, in Nagendra K. N., Stenflo J. O., eds, Proc. 2nd Int. Workshop on Solar Polarization, Bangalore, India, 1998, Kluwer Acad. Publ. ASSL 243, 515
Piskunov N., Kupka F., 2000, ApJ, submitted
Przybylski A., 1961, Nat, 189, 739
Relyea L. J., Kurucz R. L., 1978, ApJS, 37, 45
Ryabchikova T., Adelman S. J., Weiss W. W., Kuschnig R., 1997a, A&A, 322, 234
Ryabchikova T., Landstreet J. D., Gelbmann M. J., Bolgova G. T., Tsymbal V. V., Weiss W. W., 1997b, A&A, 327, 1137
Ryabchikova T., Piskunov N., Savanov I., Kupka F., Malanushenko V., 1999, A&A, 343, 229
Ryabchikova T. A., Savanov I. S., Hatzes A. P., Weiss W. W., Handler G., 2000a, A&A, 357, 981
Ryabchikova T. A., Savanov I. S., Malanushenko V. P., Kudryavtsev D. O., 2000b, Astron. Rep., in press
Schweighofer M. G., 1970, Thesis, University of Paris, Orsay
Smalley B., Kupka F., 1997, A&A, 328, 349
Smirnov O. M., Ryabchikova T. A., 1995, Astronomy Reports, 39, 755
Wegner G., Petford A. D., 1974, MNRAS, 168, 557
Wegner G., Cummins D. J., Byrne P. B., Stickland D. J., 1983, ApJ, 272, 646
Wickliffe M. E., Lawler J. E., 1997, JOSA, B14, 737
Wickliffe M. E., Salih S., Lawler J. E., 1994, JQSRT, 51, 545
Wiese W. L., Fuhr J. R., Deters T. M., 1996, Atomic Transition Probabilities of Carbon, Nitrogen, and Oxygen: a critical data compilation, J. Phys. Chem. Ref. Data, Mono. 7
Wolff S. C., Hagen W., 1976, PASP, 88, 119
Wyart J.-F., Blaise J., Bidelman W. P., Cowley C. R., 1997, Phys. Scripta, 56, 446

This paper has been typeset from a TEX/LATEX file prepared by the author.